ELSEVIER

Contents lists available at ScienceDirect

Radiation Physics and Chemistry

journal homepage: www.elsevier.com/locate/radphyschem





Enhancing the gamma radiation shielding performance: The impact of Bi₂O₃ and MgO nanoparticles on PMMA

Aml Almutery ^{a,b,c,*}, Wan Nordiana Rahman ^{a,b}, Faizal Mohamed ^{a,b}, Chia Chin Hua ^a, Khairunisak Abdul Razak ^d, Raizulnasuha Ab Rashid ^e, U. Rilwan ^{f,**}, M.I. Sayyed ^{g,j,k}, Yasser Maghrbi ^{h,i}

- ^a Department of Applied Physics, Faculty of Science and Technology, Universiti Kebangsaan Malaysia, 43600, UKM Bangi, Selangor, Malaysia
- b Nuclear Technology Research Centre, Faculty of Science and Technology, Universiti Kebangsaan Malaysia, 43600, UKM Bangi, Selangor, Malaysia
- ^c Physics Department, Faculty of Science and Humanities in Ad-Dawadmi, Shaqra University, Shaqra, 11911, Saudi Arabia
- d School of Materials and Mineral Resources Engineering, Engineering Campus, Universiti Sains Malaysia, 14300, Nibong Tebal, Penang, Malaysia
- ^e Centre for Diagnostic Nuclear Imaging, Universiti Putra Malaysia, 43400, Serdang, Selangor, Malaysia
- f Department of Physics, Faculty of Natural and Applied Sciences, Nigerian Army University, P.O. Box 1500 Biu, Borno State, Nigeria
- ^g Department of Physics, Faculty of Sciences, Isra University, Amman, Jordan
- ^h Université Côte d'Azur, 06100, Nice, France
- ¹ College of Arts & Sciences, Gulf University for Science and Technology, Hawally, Kuwait
- Renewable Energy and Environmental Technology Center, University of Tabuk, Tabuk, 47913, Saudi Arabia
- k Department of Physics and Technical Sciences, Western Caspian University, Baku, Azerbaijan

ARTICLE INFO

Handling Editor: Dr. Chris Chantler

Keywords PMMA Bi₂O₃ MgO

LAC TF

RPE

Gamma radiation

ABSTRACT

This work investigated the gamma radiation shielding performance of different nano-composites (pure PMMA, PMMA doped with Bi_2O_3 , PMMA doped with MgO, and PMMA doped with Bi_2O_3 –MgO) using the solution casting method. The experimental linear attenuation coefficients (LACs) of the samples were determined using a sodium iodide (NaI) detector and the results were compared with Phy-X theoretical results, where better matching was observed. At 59.5 keV, the PMMA doped with Bi_2O_3 sample had the largest LAC of 0.759 cm $^{-1}$ when compared to the PMMA doped with Bi_2O_3 –MgO sample with a LAC of 0.695 cm $^{-1}$. At the same energy (59.5 keV), the radiation protection efficiency of the PMMA doped with Bi_2O_3 sample was 31.34 %, which was far greater compared to that of the PMMA doped with Bi_2O_3 –MgO sample, thus confirming the PMMA doped with Bi_2O_3 sample as the optimum candidate to be applied for protection against gamma radiation.

1. Introduction

In terms of the hazardous effect of some diagnostic tools, such as X-ray machines and scanners, medical personnel recommend radiation protection for patients in order to reduce direct exposure to radiological dangers such as skin cancer, brain cancer, leukemia, mutation, and other radiation sicknesses, with this protection acting as a barrier to reduce scattered radiation from patients and leakages from other sources (Mazrani et al., 2007; Klein et al., 2009; Johnson and Cember, 2017; Charkiewicz and Backstrand, 2020; Krzywy et al., 2010; Wani et al., 2015; Dignam et al., 2019; Adlienė et al., 2020; Mittal, 2015). Other

ways of reducing exposure to radiological hazards involve reduced exposure time and increased distance. Lead is historically known as the primary shielding material, but it is toxic and heavy (Sayyed et al., 2022; Li et al., 2018; AbuAlRoos et al., 2019; Wasel and Freeman, 2018).

Lead toxicity is a general environmental health problem, affecting different systems and organs of the body. Lead ingested from food and dust used to cause serious developmental delays in infants and other health problems (El-Khatib et al., 2019; Li et al., 2017; Azman et al., 2013; Abu-Saleem et al., 2021; Ravneet et al., 2020; Kucuk et al., 2013). The Institute for Health Metrics and Evaluation reported that lead exposure causes 900,000 deaths annually. Advanced nano-technology is

E-mail addresses: aaalmutairi@su.edu.sa (A. Almutery), rilwan.usman@naub.edu.ng (U. Rilwan).

https://doi.org/10.1016/j.radphyschem.2025.113070

^{*} Corresponding author. Department of Applied Physics, Faculty of Science and Technology, Universiti Kebangsaan Malaysia, 43600, UKM Bangi, Selangor, Malaysia.

^{**} Corresponding author.

required to produce lead-free composite materials as non-toxic alternatives that are safe and eco-friendly, especially in the context of radiation protection (Pituru et al., 2020; Rilwan et al., 2024, 2025a; Almuqrin et al., 2024a, 2024b; Alasali et al., 2024). These materials can offer enhanced mechanical stability, flexibility, and radiation absorption. Nano-fillers improve photon interactions through uniform dispersion and a high surface-to-volume ratio, outperforming micro-fillers (Mostafa et al., 2022; Subedi and Lamichhane, 2023). Nano-composites such as high-density polyethylene (HDPE)/CdO and epoxy/Ga₂O₃ provide superior shielding abilities, particularly at weak photon energies. In this manner, these materials are transforming radiation shielding in the healthcare and industrial fields (Sayyed et al., 2024a, 2024b, 2024c; Rotkovich et al., 2024; Ahmed et al., 2024; Yasmin et al., 2024; Alshahri et al., 2021).

Nano-fillers incorporated into polymer materials and polycarbonate are used in radiation protection applications. The increase in the density of fillers like Bi₂O₃ improves the absorption coefficient, particularly at weak-to-medium photon energies; for example, low-density polyethylene (LDPE)/Bi₂O₃ composites with 15 % filler obstructed 80 % of X-rays at 47.9 keV effective (Ambika et al., 2017a, 2017b; Rilwan et al., 2025b, 2025c; Mehrara et al., 2021; Cao et al., 2020). Due to the small size and uniform distribution of nano-fillers, they significantly improve radiation protection by enhancing photon interactions and electron density (Abbas et al., 2022; Pavlenko et al., 2019; More et al., 2021; Berger et al., 2010; Idris et al., 2025; Rilwan et al., 2025d; Khalid et al., 2025). The comparison of micro- and nano-composites consistently shows higher absorption coefficients; for example, styrene-butadiene (SR)/Bi₂O₃ nano-composites outperformed their micro-counterparts across various energies, demonstrating the pivotal function of filler size and distribution in optimizing protection effectiveness (Tokar et al., 2013; Shahzad et al., 2022; Saleh et al., 2024; Alresheedi et al., 2023).

Bismuth oxide is an alternative to lead due to its shielding properties and non-toxicity. Various polymer materials, such as epoxy and silicon resin, confirm the efficacy of bismuth oxide nano-composites in absorbing gamma- and X-rays across the different energy ranges used in radiation shielding (Alsafi et al., 2024; Hannachi et al., 2024; Adaikalam et al., 2024; Alothman et al., 2021; Aloraini et al., 2023).

Advanced production processes, such as melt-mixing and solution casting, help in the preparation of polymer nano-composites with optimal characteristics. These methods, combined with characterizations like SEM and XRD, also improve the development of morphological and crystalline features, representing a potential innovative approach in materials improvement. These techniques explain the potential in radiation shielding (Muthamma et al., 2021; Khrenov et al., 2007; Stelzig et al., 2008; Demirbay et al., 2019; Alkan et al., 2018).

In the current research, we delved in to the fabrication of PMMA-Bi $_2$ O $_3$ –MgO thin films using the solution casting technique. The radiation shielding ability of the fabricated samples was evaluated with the aid of gamma spectrometric analysis with the Co-60, Cs-137, and Am-241 radiation sources, which are important in radiation therapy as well as medical imaging. The present study also investigated the morphology and crystal integrity of the samples via scanning electron microscopy (SEM) and X-ray diffraction (XRD) techniques in order to provide additional knowledge on the structural characteristics of the fabricated PMMA-Bi $_2$ O $_3$ -MgO thin-film samples, which brings out the potentiality of the PMMA-Bi $_2$ O $_3$ -MgO thin films in resolving the problem of lead toxicity in terms of radiation shielding applications.

2. Material and methods

2.1. Preparation of the PMMA/nano-composites

The preparation of transparent poly (methyl methacrylate) (PMMA) entailed dissolving 20 g of PMMA (with the chemical formula $C_5H_8O_2$) in $160~\text{cm}^3$ of chloroform (CHCl $_3$) using a magnetic stirrer for one day, while gradually adding 0.01~g of bismuth and magnesium oxides in 5

cm³ of chloroform. The nanoparticle-impregnated PMMA polymer was poured into an aluminum dish and allowed to remain at room temperature for approximately four days for the solvent to slowly cool in order to ensure thin-film formation (Alkan et al., 2018). The masses of the fabricated circular samples were individually measured with the aid of a digital weighing balance (SF-400) which has a precision of ± 0.1 . the volume of the circular samples was calculated using the formula for volume of circle as described in Eq. (1) (Rilwan et al., 2025c). The measured masses and the calculated volumes were then utilized to calculate the densities (in g/cm³) of the samples as described in Eq. (2) (Rilwan et al., 2025a). The sample's chemical compositions in wt.%, as well as the density of the fabricated PMMA nano-composites in g/cm³ are presented in Table 1.

$$V = \left(\frac{4}{3}\right) \times \pi \times r^3 \tag{1}$$

$$\rho = \frac{M}{V} \tag{2}$$

where the mass of each sample is represented by M, the volume denoted by V, and r stands for radius of the circle.

2.2. Characterization

In this research, XRD (Bruker AXS Germany Brand and D8 advance Model) was utilized to investigate the structural characteristics of the fabricated samples. ICDD standards (the reference diffraction pattern often utilized during the XRD analysis of samples in order to identify the phases of the crystalline materials) were maintained in the XRD device (using Cu-Kα radiation) with a wavelength of 1.54 A°, step size of 0.02°, and scan speed of 1°/min under ambient temperature, where a 2 h spectrum was used between 10 and 80° (0) for the thin films. SEM with 5–20 kV accelerating potential, high-vacuum mode, secondary electron detector, and a gold sputter coating for the non-conductive samples was employed to check the surface morphology of the fabricated samples. The molecular structure and composition of the samples were analyzed using Fourier transform infrared (FITR) spectroscopy (PerkinElmer Brand and FTIR Spectrum-400 Model) at the wavelength spectrum of 400–4000 cm⁻¹, with a resolution of 4/cm and utilizing the attenuated total reflectance (ATR) pellet technique at normal (room) temperature (Alkan et al., 2018).

2.3. Radiation attenuation evaluation

A sodium iodide (NaI) detector was employed, having an efficiency of 10–20 % for the identification of the γ -spectrum emitted from the Am-241 (59.5 keV) γ -sources, 5–15 % for the identification of the γ -spectrum emitted from the Co-60 (1173.2 and 1332.5 keV) γ -sources, and 10–25 % for the identification of the γ -spectrum emitted from the Cs-137 (661.6 keV) γ -sources (Rilwan et al., 2025b). The narrow beam method was employed in the experimental measurements, where a lead collimator was placed between the source and the detector, as shown in Fig. 1. The PMMA/nano-composite sample was placed in a measured position between the detector and the source, with the gamma intensity taken in the absence (I_0) and presence (I_x) of the sample. The data for the

Table 1 Chemical compositions of the developed nano-composites in wt.%.

Sample Code	CHCl ₃	$C_5H_8O_2$	Bi2O3	MgO	Density (g/cm ³)
Pure PMMA	0.920	0.0777	0.0000	0.0000	1.837
PMMA/Bi ₂ O ₃	0.920	0.07757	0.0021	0.0000	1.836
PMMA/MgO	0.920	0.07757	0.0000	0.0021	1.772
PMMA/Bi ₂ O ₃ :MgO	0.920	0.0774	0.0021	0.0021	1.698

 $CHCl_3 = chemical$ formula for chloroform; $C_5H_8O_2 = chemical$ formula for poly (methyl methacrylate) (PMMA).

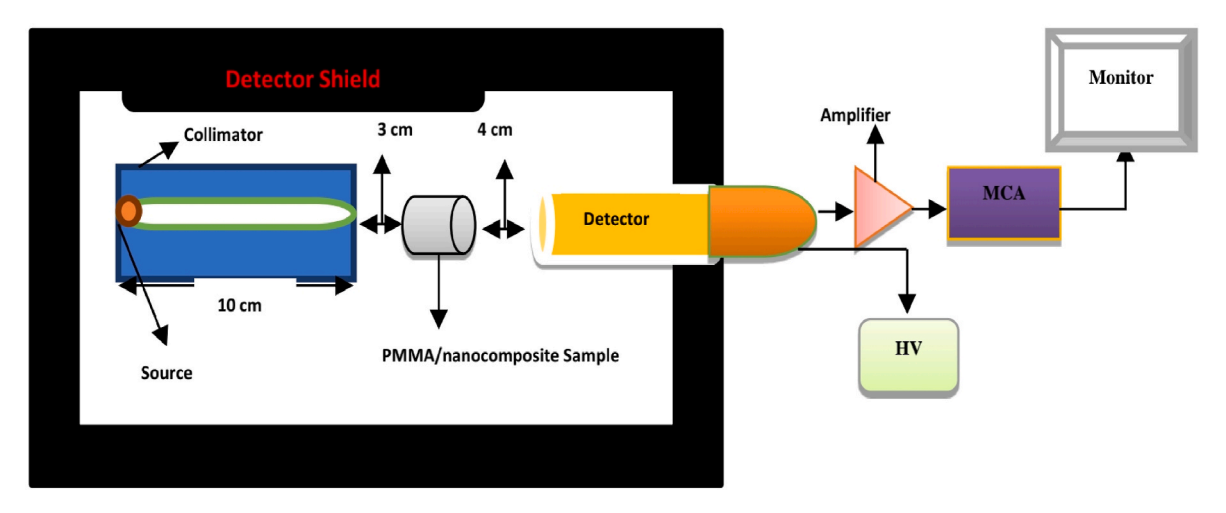


Fig. 1. Setup for the experimental measurement.

intensity was used with the aid of Eq. (3) (Aloraini et al., 2023, Cağlar et al., 2019; Yousefi et al., 2023) to evaluate the experimental linear attenuation coefficient (LAC) in ${\rm cm}^{-1}$, as presented in Table 2.

$$LAC = \frac{1}{X} \ln \left(\frac{I_0}{I} \right) \tag{3}$$

where x is the thickness of the thin films in cm, I is the intensity in count per seconds (cps) with the presence of the PMMA nano-composite, and Io the is intensity also in cps but without the presence of the PMMA nano-composite. Moreover, the mass attenuation coefficients (MACs) of our samples in cm²/g were examine using Eq. (4) (Aloraini et al., 2023; Krishnamoorthy et al., 2012; Boubeta et al., 2010; Chalkidou et al., 2011; Di et al., 2012).

$$\mu_{m} = \frac{\mu}{\rho} = \sum w_{i} \left(\frac{\mu}{\rho}\right)_{i} \tag{4}$$

where, w_i represents the weight fraction, and $\left(\frac{\mu}{\rho}\right)_i$ stands for the MAC for an individual element in the compound. The half value layer (HVL, cm), as determined in Eq. (5), indicates the shield thickness required to reduce the radiation beam intensity to one-half, while the tenth value layer (TVL, cm) computed from Eq. (6) denotes the shield layer needed to minimize the radiation beam intensity to one-tenth of the initial level (Muthamma et al., 2021; Demirbay et al., 2019; Saudi et al., 2021; Gohil et al., 2017; Müller et al., 2017; Deka et al., 2022).

$$HVL = \frac{\ln 2}{\mu} \tag{5}$$

$$TVL = \frac{\ln 10}{\mu} \tag{6}$$

The mean free path (MFP, cm), given by Eq. (7), shows the average distance at which a photon travels through the medium of a given sample before interacting with its material (Alkan et al., 2018; Bawazeer et al., 2023; Ali et al., 2015a; Agar, 2018; Eke et al., 2017; Kavun et al., 2019).

$$MFP = \frac{1}{\mu} \tag{7}$$

The transmission factor (TF, %), the radiation protection efficiency (RPE, %), and the effective atomic number (Z_{eff}) in this work were calculated via Eqs. (8)–(10), respectively (Surung et al., 2016).

$$TF = \frac{I}{I_0} = e^{-\mu x} \tag{8}$$

$$RPE = 1 - TF \tag{9}$$

$$Z_{eff} = \frac{\delta_a}{\delta_e} \times \frac{Q_a}{\sigma} \tag{10}$$

The electronic and atomic cross-sections (cm²/g) are given as δ_e and δ_a , the mass number of the atom (g/mol) is denoted by Qa, while the density is represented by σ . The values for δ_e and δ_a were obtained from Eqs. (11) and (12), respectively (Rilwan et al., 2025c).

$$\delta_a = \frac{\delta_t \times P_a}{Q_a \times \sigma} \tag{11}$$

$$\delta_e = \frac{\delta_t \times P_e}{Q_e \times \sigma} \tag{12}$$

where δt represents the overall cross-section (cm²), Pa stands for Avogadro's number (6.02 x10²³ mol⁻¹), Pe indicates the number of electrons per unit atom, and Qe is the electron mass (g).

3. Results and discussion

The XRD of the pure PMMA, PMMA/Bi₂O₃, PMMA/MgO, and PMMA/Bi₂O₃:MgO samples are depicted in Fig. 2. An amorphous character with a large diffraction peak of $2\theta = 30^{\circ}$ was observed from the PMMA samples in the XRD pattern, and particularly in the pure PMMA sample (see Fig. 2). There are no distinct and sharp peaks observed in the PMMA samples, which resulted in poor arrangement of

 Table 2

 Linear attenuation coefficient for experimental and theoretical data.

Energy (keV)	Pure PMMA		PMMA/Bi ₂ O ₃	PMMA/Bi ₂ O ₃		PMMA/MgO		PMMA/Bi ₂ O ₃ :MgO	
	Exp (cm ⁻¹)	The (cm ⁻¹)	Exp (cm ⁻¹)	The (cm ⁻¹)	Exp (cm ⁻¹)	The (cm ⁻¹)	Exp (cm ⁻¹)	The (cm ⁻¹)	
59.5	0.701	0.734	0.744	0.752	0.703	0.709	0.688	0.695	
661.6	0.112	0.139	0.131	0.140	0.132	0.135	0.125	0.129	
1173.2	0.103	0.106	0.100	0.106	0.103	0.102	0.094	0.098	
1332.5	0.091	0.099	0.095	0.099	0.092	0.096	0.090	0.092	

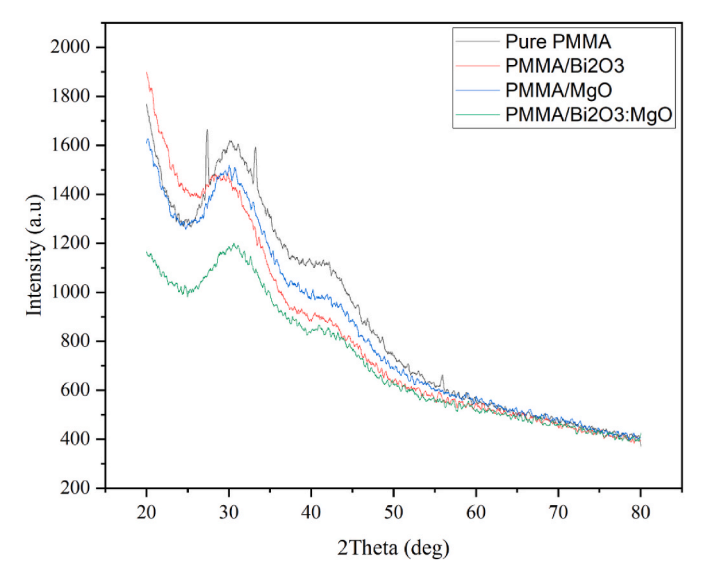


Fig. 2. The XRD spectra of pristine PMMA and the produced PMMA/Bi $_2$ O $_3$, PMMA/MgO, and PMMA/Bi $_2$ O $_3$:MgO nano-composites at filler loadings of 0 %, 2.5 %, 2.5 %, and 5 %, respectively.

the atoms in the sample and in turn could affect the crystal structure of the material. A long-ranged pattern was noticed in the samples due to the wide halo centered at $2\theta=27-33^{\circ}$, signifying the lack of long-range order as documented in Mazrani et al. (2007) and Klein et al. (2009). The peaks at $40-45^{\circ}$ correspond to MgO and Bi₂O₃ crystalline phases,

which indicates their existence in the fabricated PMMA composite. The XRD pattern of PMMA dopped with 2.5 wt% of Bi_2O_3 , 2.5 wt% of MgO, and 5 wt% of Bi_2O_3 :MgO nanoparticles were observed to match with the ICDD PDF card number of #00-045-0566 corresponding to Bi_2O_3 and #00-045-0946 corresponding to MgO. The presence of $\frac{20}{3}$ with the ICDD PDF card number of ending to MgO. The presence of $\frac{20}{3}$ with the indicate $\frac{20}{3}$ show that apparently no strong chemical reaction took place between the Bi_2O_3 .

MgO, and the PMMA, but rather the metal oxides maintained their crystal structures, confirming the nanoparticles' uniform dispersion within the PMMA matrix. Moreover, such characteristic is evidence that the interaction is restricted to physical dispersion as well as possibly Lewis's acid-base interaction at the PMMA–oxide interface. The variation of diffraction patterns is in line with those reported in studies on PMMA application (Surung et al., 2016).

Based on the SEM analysis of the synthesized samples, a smooth distribution of the $\rm Bi_2O_3$ and MgO nanoparticles was observed in all samples, as presented in Fig. 3(a–d). The surfaces in Fig. 3a, b, and 3c indicate that the protrusions from the implanted nanoparticles in the composite material are distinctly visible, whereas the image in Fig. 3d displays flat surfaces for the PMMA/Bi₂O₃:MgO sample. The smooth surface morphology seen in Fig. 3d indicates that the Bi₂O₃:MgO are well-accelerated within the PMMA matrix, which reduces the agglomeration of nanoparticles (Krzywy et al., 2010; Wani et al., 2015; Zhou and Shang, 2023) due to the firm interfacial interactions (Dignam et al., 2019; Ali et al., 2015b).

Base on the EDX results in Fig. 3(a–d), the concentration of Mg and Bi are found to be high, donating to the density of the nano-particle in all samples, with MgO causing the uniform dispersion while $\rm Bi_2O_3$ improving the contrast at the surface because of its superior proton number. This tells the reason why the sample's SEM images exhibited

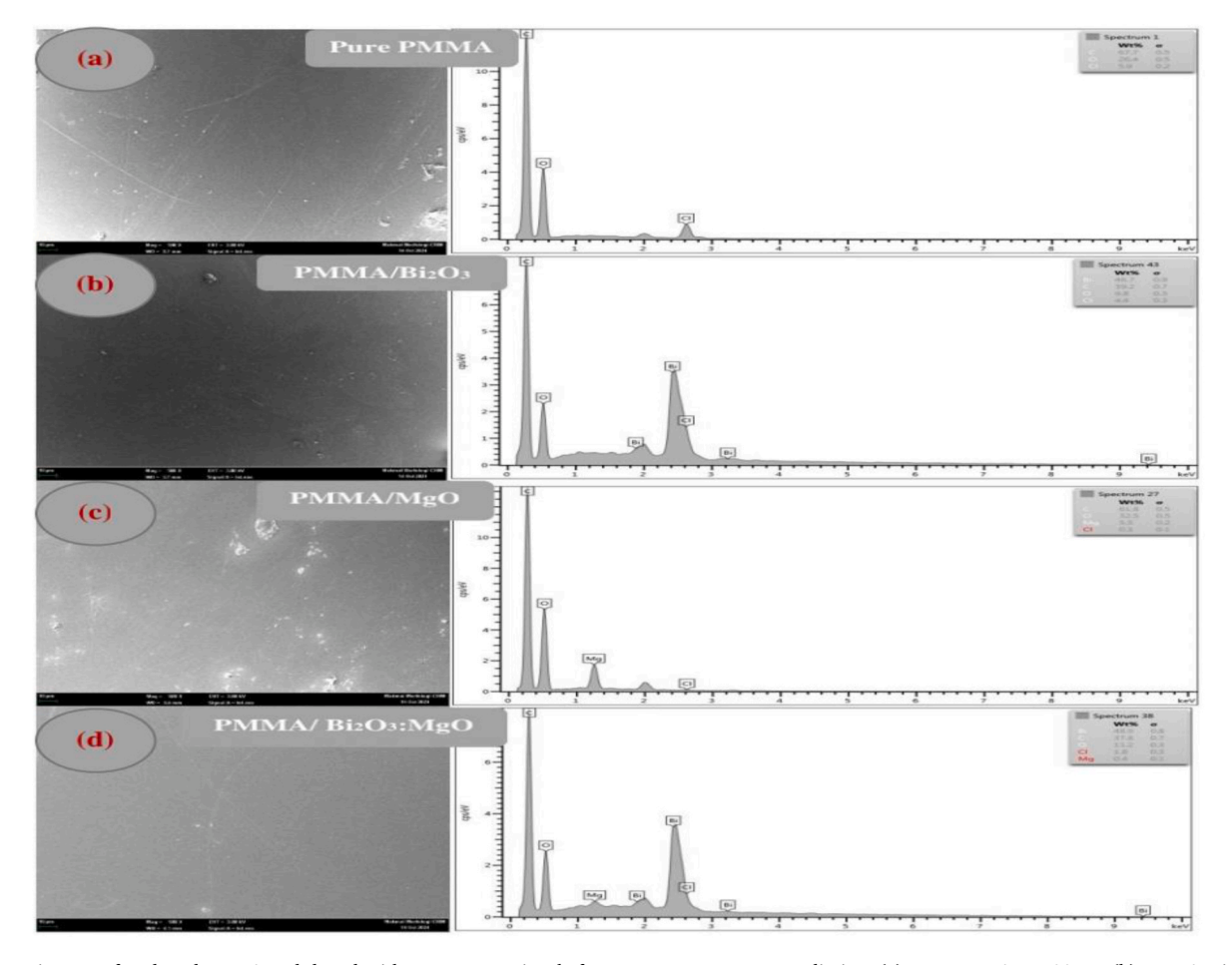


Fig. 3. SEM images of undoped PMMA and doped with nano-composites before exposure to gamma radiation: (a) pure PMMA at $500 \times$, (b) PMMA/Bi₂O₃ nano-composite sample, (c) PMMA/MgO nano-composite sample, (d) PMMA/Bi₂O₃:MgO nano-composite sample.

smooth surfaces and less agglomeration (Rilwan et al., 2025c).

Figs. 4, 5, 6, and 7 respectively present the FTIR spectra of pure PMMA, PMMA doped with Bi₂O₃, PMMA doped with MgO, and PMMA co-doped with Bi₂O₃-MgO, which give a specific peak that represents the functional grouping similar to PMMA. At 1720 cm⁻¹, the prominent peak of pure PMMA matches the ester grouping stretching vibrations (C=O), whereas the peaks that fall within 2950-3000 cm⁻¹ show stretching vibrations (C–H). The stretching, C–O–C, closely corresponds to the absorption peak at 1150-1250 cm⁻¹. Fig. 4 demonstrates the absence of additional peaks, indicating the lack of doping, which emphasizes the structural baseline of pure PMMA based on the report of Bijanu et al. (2022). The PMMA doped with Bi₂O₃ sample in Fig. 5 shows an appreciable peak at 17200 cm⁻¹, which confirms the interaction of the ester group of PMMA with Bi₂O₃, with a slight drift observed in the wavenumber, confirming modification in the bond due to the high proton number of the Bi₂O₃, in agreement with the results of Mehrara et al. (2021). The PMMA doped with MgO reveals a maximum peak value around 1142 cm⁻¹, as seen in Fig. 6, indicating a shift in the C=O and C-H bonds, which could enhance the molecular interactions of the tested materials, aligning with the results reported by Mehrara et al. (2021) and Park and Hwang (2017). The Bi₂O₃-MgO co-doped PMMA, as shown in Fig. 7, indicates a drifted absorption peak, specifically in C=O stretching, with prominent peaks resulting from Bi₂O₃ and MgO, in alignment with the report of Hashem et al. (2017). For example, in Fig. 6, some prominent peaks occur at 1723 and 752 cm⁻¹, while the same peaks in Fig. 7 occur at 1725 and 748 cm⁻¹, respectively, indicating a slight drift.

Based on Fig. 8, the LACs for the pure PMMA determined theoretically and experimentally show extremely high values (0.734 cm⁻¹ theoretically and 0.701 cm⁻¹ experimentally) at the lowest energy level considered in this research (59.50 keV). This considerable attenuation at the least energy could be due to the photoelectric interaction being the predominant interaction at lower energy levels where the tendency of interaction is higher. There is a sharp drop in the LAC values (0.099 cm⁻¹ theoretically and 0.091 cm⁻¹ for the experimental data) as the energy reaches 1332.5 keV, which could be associated with the Compton scattering influence, since at regions where Compton scattering is dominant, the interaction between the incoming photons and the absorbing samples is reduced. Based on the results, a strong agreement exists between the experimental and theoretical values; for example, at 1173.20 keV the experimental LAC value is 0.103 cm⁻¹ while the theoretical LAC shows a value of $0.106~{\rm cm}^{-1}$. This result agrees with that of Hashem et al. (2017). The LAC falls as the energy raises in the 59.5-1332.5 keV range, with the PMMA/Bi₂O₃ sample consistently retaining the highest attenuation coefficient due to the presence of Bi₂O₃ (Bijanu et al., 2022). The LAC values of the pure PMMA, PMMA/MgO,

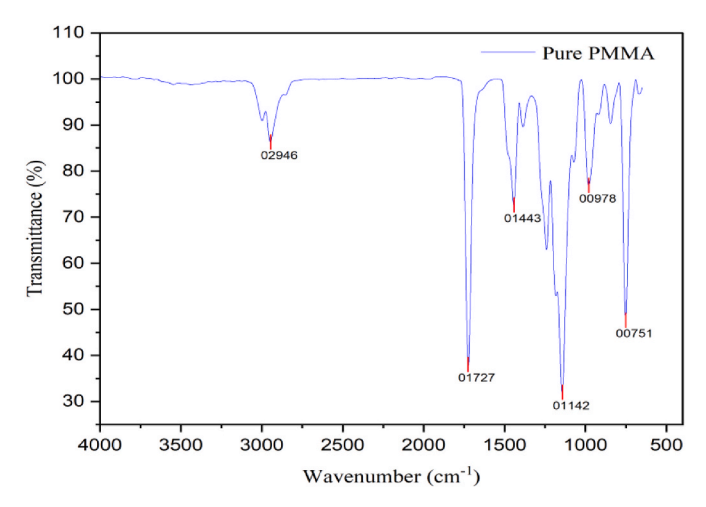


Fig. 4. FTIR spectra for pure poly (methyl methacrylate) (PMMA).

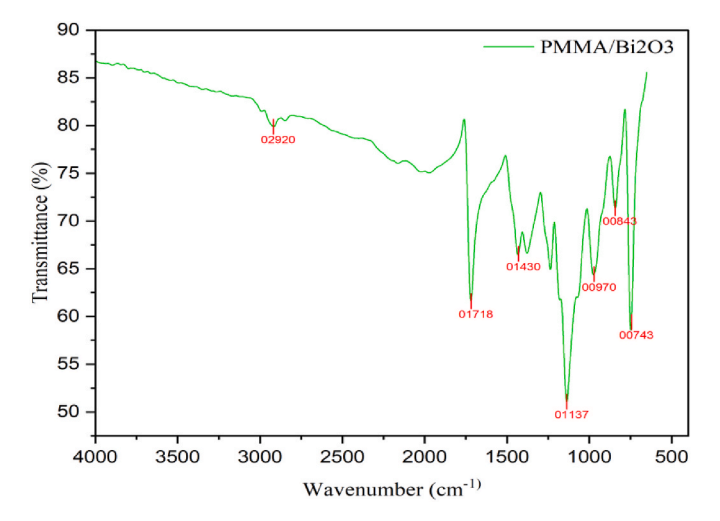


Fig. 5. FTIR spectra for PMMA doped with Bi₂O₃.

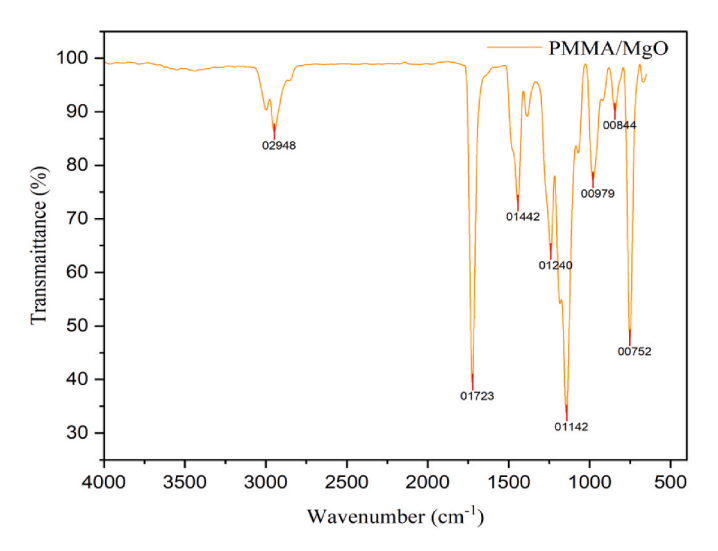


Fig. 6. FTIR spectra for PMMA doped with MgO.

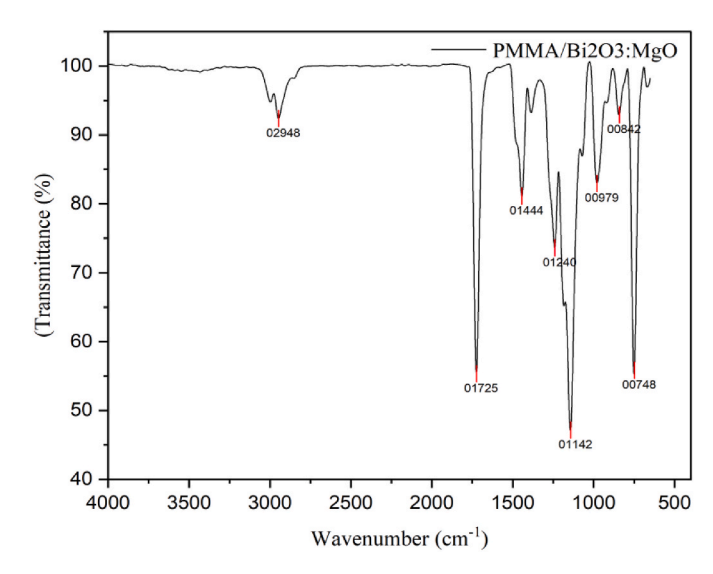


Fig. 7. FTIR spectra for PMMA doped with Bi₂O₃ and MgO.

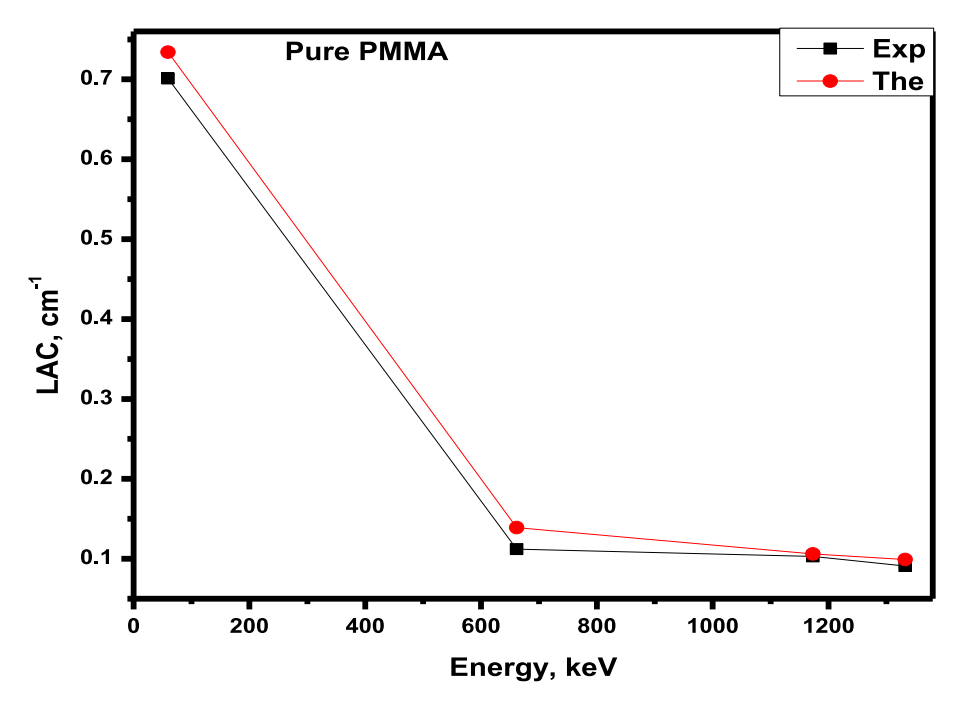


Fig. 8. A comparison chart showing the linear attenuation coefficient (LAC) for pure PMMA determined theoretically and experimentally as a function of the radiation's energy (E) in keV.

PMMA/Bi $_2O_3$, and PMMA/Bi $_2O_3$:MgO samples respectively drop from 0.701 to 0.091, 0.744 to 0.095, 0.703 to 0.092, and 0.688 to 0.09 cm $^{-1}$, indicating a similar percentage decrease of 13 %, 12.76 %, 13.09 %, and 13.09 %, respectively, and thus confirming the PMMA/Bi $_2O_3$ and PMMA/Bi $_2O_3$:MgO samples as promising candidates for radiation shielding applications.

Fig. 9 presents a chart showing (a) the MACs for all the studied samples against energy (E) in keV, and (b) a chart of the MACs of all the samples at 59.5 keV. In Fig. 9a, the pure PMMA and PMMA/MgO samples show extremely low MACs at 59.50 keV with respective values of 0.3996 and 0.4001 cm 2 /g, compared to the PMMA/Bi₂O₃:MgO and PMMA/Bi₂O₃ samples that exhibit high respective values at 0.4001 and

0.4096 cm²/g. The raise in MAC values for the PMMA/Bi $_2$ O $_3$:MgO and PMMA/Bi $_2$ O $_3$ samples could be as a result of the presence of Bi $_2$ O $_3$. As the energy increases from 59.5 to 1332.5 keV for the pure PMMA, PMMA/MgO, PMMA/Bi $_2$ O $_3$, and PMMA/Bi $_2$ O $_3$:MgO samples, the MAC experiences a significant average drop by 82.6 %, 85.9 %, and 87.075 %, respectively, at 661.6, 1173.2, and 1332.5 keV, as shown in Table 3. Since the drop is the maximum at 1332.5 keV and the minimum at 59.5 keV, it is confirmed that the superiority of the studied composite is significant at the low energy of 59.5 keV, while negligible at the high energies of 661.6, 1173.2, and 1332.5 keV. Similar MAC values were observed across the pure PMMA and PMMA/MgO samples, as well as the PMMA/Bi $_2$ O $_3$ and PMMA/Bi $_2$ O $_3$:MgO samples, as presented in Fig. 9b.

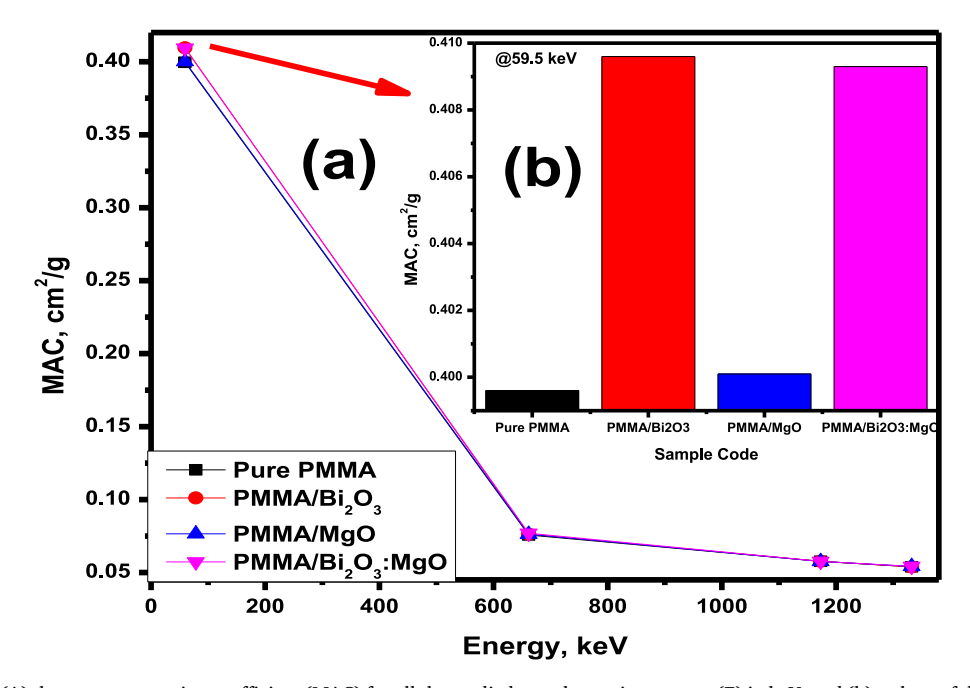


Fig. 9. A chart showing (A) the mass attenuation coefficient (MAC) for all the studied samples against energy (E) in keV, and (b) a chart of the MACs of all samples at 59.5 MeV.

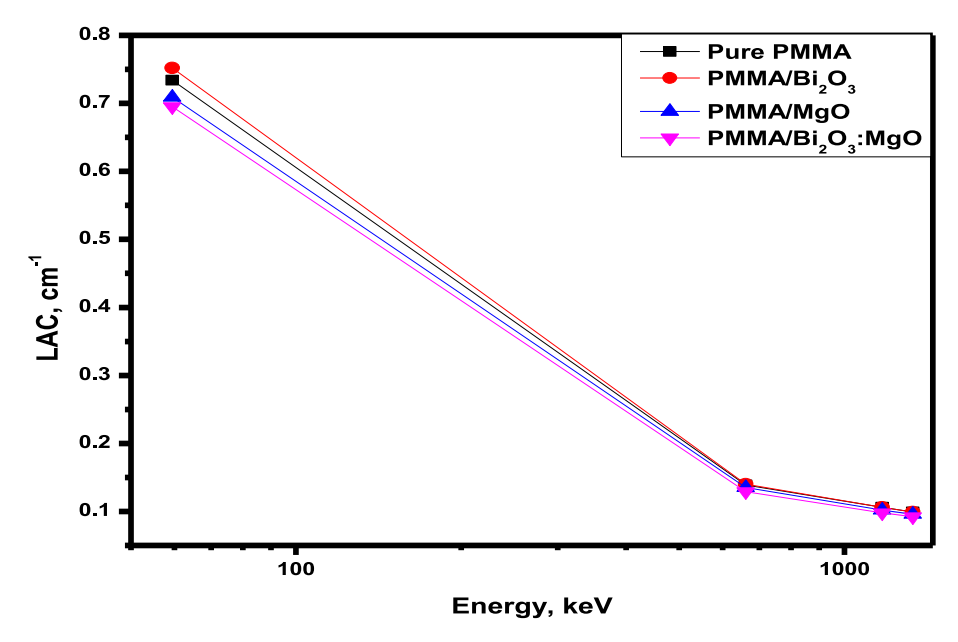


Fig. 10. A comparison chart showing the LAC for all the studied samples as a function of energy (E) in keV.

Table 3
The percentage drop in MAC (%).

Energy (keV)	Percentag	Percentage Drop in MAC (%)				
	Pure PMMA	PMMA/ Bi ₂ O ₃	PMMA/ MgO	PMMA/ Bi ₂ O ₃ :MgO	Drop	
59.5	0.00	0.00	0.00	0.00	0.0000	
661.6	84.0	83.4	81.2	81.8	82.600	
1173.2	85.3	86.7	85.3	86.3	85.900	
1332.5	87.0	87.4	87.0	86.9	87.075	

Even though the PMMA/ $\mathrm{Bi}_2\mathrm{O}_3$ and PMMA/ $\mathrm{Bi}_2\mathrm{O}_3$:MgO samples show an equal percentage decrease, the reduction in MAC values observed as the energy raised could be attributed to a reduction in the probability of interaction as the energy leaves the photoelectric region towards the Compton scattering region (Rilwan et al., 2025e) (see Fig. 10).

At the 661.6 keV energy level, the HVL, TVL, and MFP are the least in the PMMA/Bi $_2$ O $_3$ sample with respective values of 4.95, 16.44, and 7.14 cm, as shown in Fig. 11, while the PMMA/Bi $_2$ O $_3$:MgO sample respectively has values of 5.37, 17.85, and 7.75 cm for the HVL, TVL, and MFP. The least HVL, TVL, and MFP values at 661.6 keV energy seen in the PMMA/Bi $_2$ O $_3$ sample could be due to the presence of Bi $_2$ O $_3$, which improves the sample's density, while the high values of the radiation

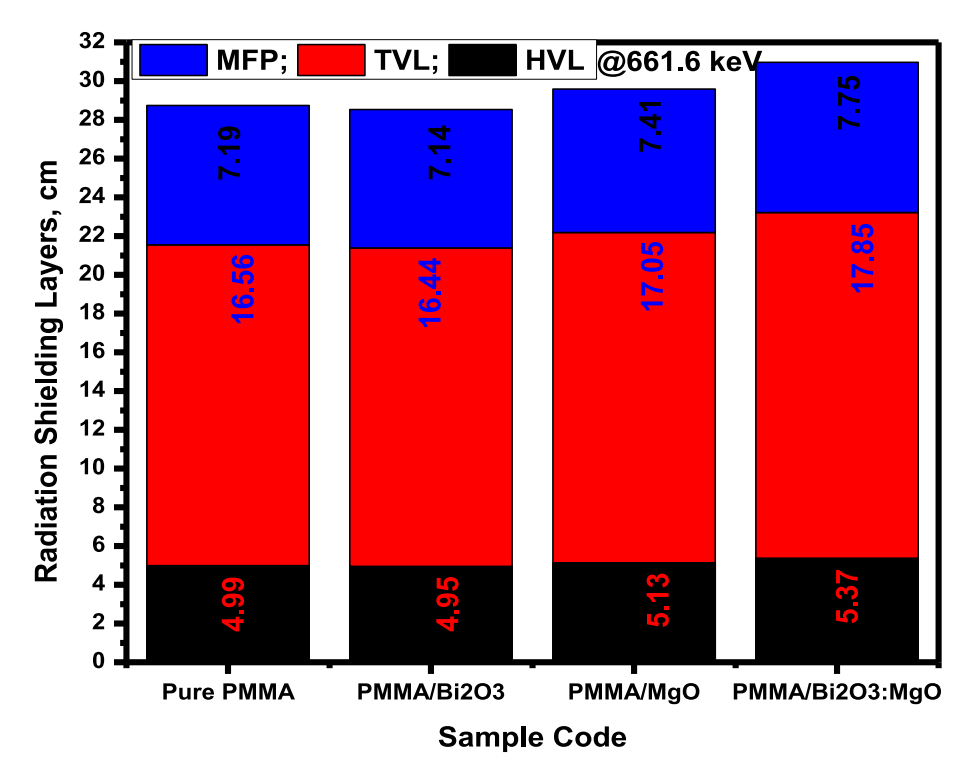


Fig. 11. A comparison chart showing the results of the radiation shielding layers for all the samples at energy (E) of 661.6 keV.

shielding layers seen in the PMMA/Bi₂O₃:MgO sample could be related to the presence of MgO which has a low atomic number, thus reducing the density of the resulting sample. Since materials with high values for the radiation shielding layers exhibit poorer attenuation, it is confirmed that the PMMA/Bi₂O₃ sample possesses the optimum shielding performance compared to the other examined samples in this study. This result agrees with the report of Bijanu et al. (2022).

As seen in Fig. 12, the RPE of the PMMA/Bi₂O₃, pure PMMA, PMMA/MgO, and PMMA/Bi₂O₃:MgO samples respectively reduce from 0.3134 to 0.0676 %, 0.3072 to 0.0671 %, 0.2985 to 0.0653 %, and 0.2935 to 0.0625 % as the energy decreases from 59.5 to 1332.5 keV, with the PMMA/Bi₂O₃ sample maintaining the highest RPE throughout the tested energy range. The reduction observed in RPE as the energy increases could be due to the decrease in the number of interactions at the higher energy range. This shows a similar trend to the one reported by Bijanu et al. (2022).

In Fig. 13, the Z_{eff} also shows a similar trend to the LAC, as it also decreases with increased energy, showing that the Compton scattering interaction is the dominant interaction that takes place at the higher energy range. The PMMA/Bi $_2O_3$ sample shows the highest Z_{eff} values due to the presence of Bi_2O_3 , while the PMMA/Bi $_2O_3$:MgO sample exhibits the least Z_{eff} value due to the presence of MgO, confirming the PMMA/Bi $_2O_3$ sample as the preferred candidate for the attenuation of gamma radiation. This result agrees with that reported in Yousefi et al. (2023).

4. Conclusion

In the current study, all the fabricated samples were found to be amorphous in nature, which suggests that there was no structural change as the dopants (Bi₂O₃, MgO, and Bi₂O₃:MgO) were added to the PMMA matrix. This is an indication that, even with the physical mixing, there was no observed alteration in the chemical reaction of all the samples. Based on the SEM results, there was an even-spreading of the nanoparticle (Bi₂O₃) within the PMMA matrix, resulting in a smooth surface morphology. Great C=O stretching peaks of PMMA doped with Bi₂O₃ up to 17200 cm⁻¹ were reported by the FTIR analysis, confirming a rise in the interactions. At 59.5 keV, the PMMA doped with Bi₂O₃ sample had the largest LAC of 0.759 cm⁻¹ and a MAC of 0.4096 cm²/g,

when compared to the PMMA doped with Bi_2O_3 –MgO sample with a LAC 0.695 cm $^{-1}$. The PMMA doped with Bi_2O_3 sample had the least HVL and TVL of 4.95 and 16.44 cm, respectively, thus evidencing its radiation shielding superiority. The PMMA doped with Bi_2O_3 sample hence stands out as the optimum candidate for gamma radiation protection among the remaining tested samples.

CRediT authorship contribution statement

Aml Almutery: Writing - review & editing, Writing - original draft, Visualization, Validation, Supervision, Software, Resources, Project administration, Methodology, Investigation, Funding acquisition, Formal analysis, Data curation, Conceptualization. Wan Nordiana Rahman: Writing - review & editing, Writing - original draft, Visualization, Validation, Supervision, Software, Resources, Project administration, Methodology, Investigation, Funding acquisition, Formal analysis, Data curation, Conceptualization. Faizal Mohamed: Writing review & editing, Writing - original draft, Visualization, Validation, Supervision, Software, Resources, Project administration, Methodology, Investigation, Funding acquisition, Formal analysis, Data curation, Conceptualization. Chia Chin Hua: Writing – review & editing, Writing - original draft, Visualization, Validation, Supervision, Software, Resources, Project administration, Methodology, Investigation, Funding acquisition, Formal analysis, Data curation, Conceptualization. Khairunisak Abdul Razak: Writing - review & editing, Writing - original draft, Visualization, Validation, Supervision, Software, Resources, Project administration, Methodology, Investigation, Funding acquisition, Formal analysis, Data curation, Conceptualization. Raizulnasuha Ab Rashid: Writing - review & editing, Writing - original draft, Visualization, Validation, Supervision, Software, Resources, Project administration, Methodology, Investigation, Funding acquisition, Formal analysis, Data curation, Conceptualization. U. Rilwan: Writing - review & editing, Writing - original draft, Visualization, Validation, Supervision, Software, Resources, Project administration, Methodology, Investigation, Funding acquisition, Formal analysis, Data curation, Conceptualization. M.I. Sayyed: Writing - review & editing, Writing original draft, Visualization, Validation, Supervision, Software, Resources, Project administration, Methodology, Investigation, Funding acquisition, Formal analysis, Data curation, Conceptualization. Yasser

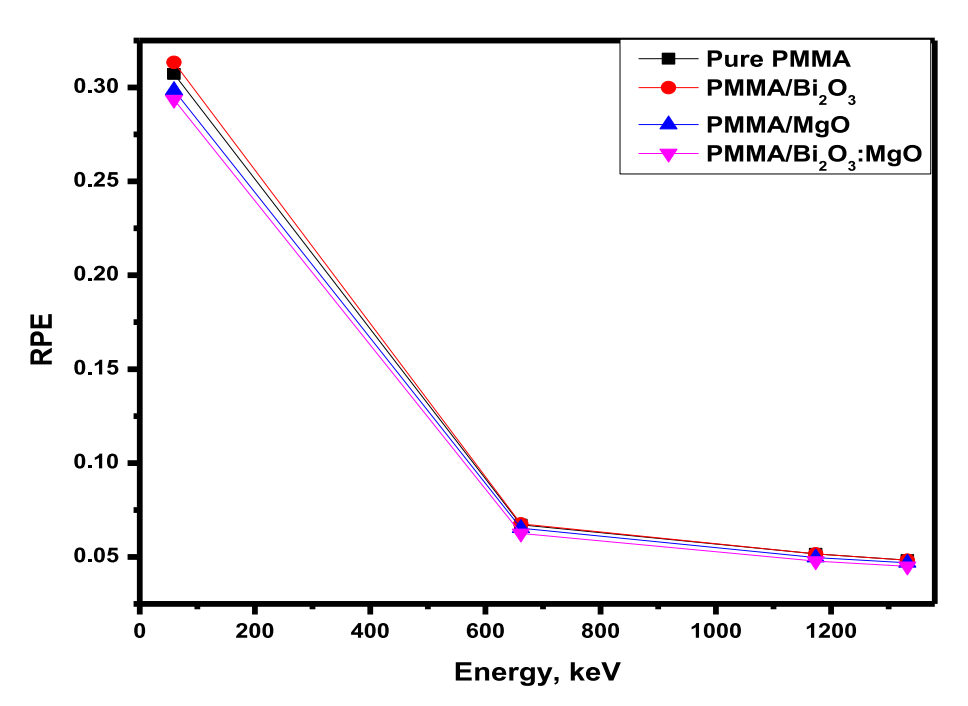


Fig. 12. A chart showing the radiation protection efficiency (RPE) for all the samples as a function of energy (E) in keV.

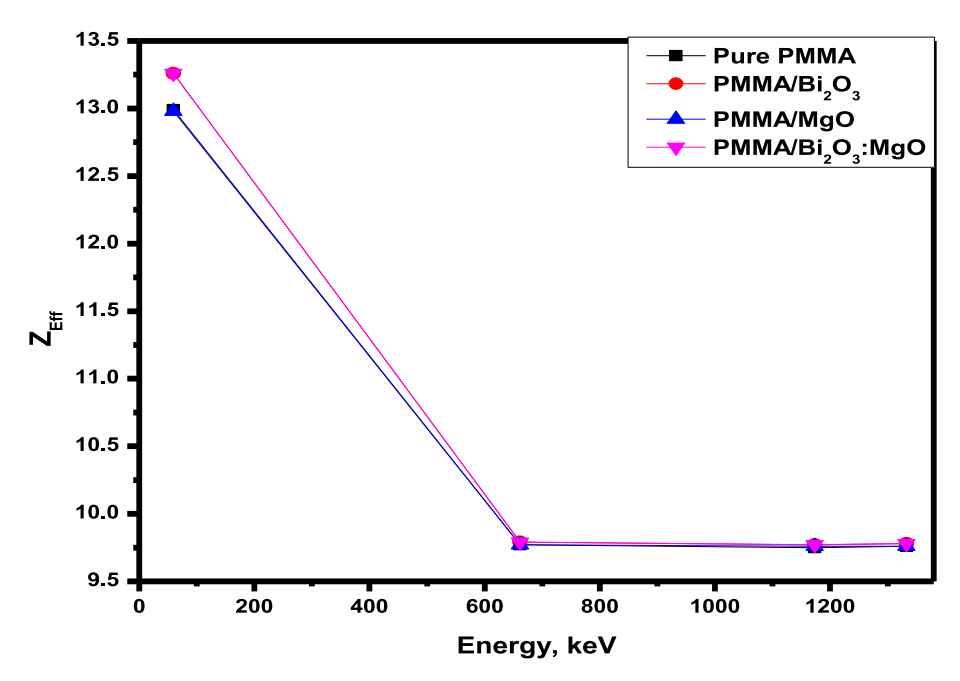


Fig. 13. A chart comparing the effective atomic number (Zeff) for all the samples as a function of energy (E) in keV.

Maghrbi: Writing – review & editing, Writing – original draft, Visualization, Validation, Supervision, Software, Resources, Project administration, Methodology, Investigation, Funding acquisition, Formal analysis, Data curation, Conceptualization.

Declaration of competing interest

The authors declare that they have no known competing financial interests or personal relationships that could have appeared to influence the work reported in this paper.

Acknowledgements

The authors would like to thank Shaqra University & Nuclear Technology Research Center (Universiti Kebangsaan Malaysia) for providing the research facilities and support.

Data availability

Data will be made available on request.

References

Abbas, M.I., El-Khatib, A.M., Dib, M.F., Mustafa, H.E., Sayyed, M.I., Elsafi, M., 2022. The influence of Bi₂O₃ nanoparticle content on the γ-ray interaction parameters of silicon rubber. Polymers 14, 1048. https://doi.org/10.3390/polym14051048.

AbuAlRoos, N.J., Baharul Amin, N.A., Zainon, R., 2019. Conventional and new lead-free radiation shielding materials for radiation protection in nuclear medicine: a review. Radiat. Phys. Chem. 165, 108439. https://doi.org/10.1016/j. radphyschem.2019.108439.

Abu-Saleem, A.R., Abdelal, N., Alsabbagh, A., Al-Jarrah, M., Al-Jawarneh, F., 2021. Radiation shielding of fiber reinforced polymer composites incorporating lead nanoparticles—an empirical approach. Polymers 13, 3699. https://doi.org/ 10.3390/polym13213699.

Adaikalam, K., Vikraman, D., Lee, D.-H., Cho, Y.-A., Kim, H.-S., 2024. Optical and UV shielding properties of inorganic nanoparticles embedded in polymethyl methacrylate nanocomposite freestanding films. Polymers 16 (8), 1048. https://doi.org/10.3390/polym16081048.

Agar, O., 2018. Study on gamma ray shielding performance of concretes doped with natural sepiolite mineral. Radiochim. Acta 106, 1009–1016. https://doi.org/ 10.1515/ract-2018-2981.

Alasali, H.J., Rilwan, U., Mahmoud, K.A., Hanafy, T.A., Sayyed, M.I., 2024. Comparative Analysis of TiO₂, Fe₂O₃, CaO and CuO in borate-based glasses for gamma ray shielding. Nucl. Eng. Technol. https://doi.org/10.1016/j.net.2024.05.006.

Adlienė, D., Gilys, L., Griškonis, E., 2020. Development and characterization of new tungsten and tantalum containing composites for radiation shielding in medicine. Nucl. Instrum. Methods Phys. Res. Sect. B Beam Interact. Mater. Atoms 467, 21–26. https://doi.org/10.1016/j.nimb.2020.01.027.

Ahmed, E.K., Mahran, H.M., Alrashdi, M.F., Elsafi, M., 2024. Studying the shielding ability of different cement mortars against gamma ray sources using waste iron and BaO microparticles. Nexus of Future Materials 1, 1–5. https://nfmjournal.com/a rticles/3.

Ali, U., Karim, K.J.B.A., Buang, N.A., 2015a. A review of the properties and applications of poly (methyl methacrylate) (PMMA). Polym. Rev. 55 (4), 678–705. https://doi. org/10.1080/15583724.2015.1031377.

Ali, H., et al., 2015b. Characterization of amorphous and crystalline structures in PMMA and its composites. J. Polym. Sci. 53 (2), 342–348.

Alkan, Ü., Kılıç, M., Karabul, Y., Çağlar, M., İçelli, O., Özdemir, Z.G., 2018. X-ray irradiated LDPE/PP blends with high mechanical and dielectric performance.
J. Appl. Polym. Sci. 135, 46571

Almuqrin, A.H., Mahmoud, K.A., Rilwan, U., Sayyed, M.I., 2024a. Influence of various metal oxides (PbO, Fe₂O₃, MgO, and Al₂O₃) on the mechanical properties and γ-ray attenuation performance of zinc barium borate glasses. Nucl. Eng. Technol. https://doi.org/10.1016/j.net.2024.02.032

Almuqrin, A.H., Sayyed, M.I., Kumar, A., Rilwan, U., 2024b. Characterization of glasses composed of PbO, ZnO, MgO, and B_2O_3 in terms of their structural, optical, and gamma ray shielding properties. Nucl. Eng. Technol. https://doi.org/10.1016/j. net.2024.02.047.

Aloraini, D.A., Elsafi, M., Almuqrin, A.H., Yasmin, S., Sayyed, M.I., 2023. Synergistic effect in ionizing radiation shielding with recent tile composites blended with marble dust and BaO micro/nanoparticles. Crystals 13, 1057.

Alothman, M.A., Al-Buriahi, M.S., Saleh, H.H., Alomairy, S., Tonguç, B.T., 2021. Polarizability, metallization criterion, and radiation attenuation performance of pure and Ag-doped poly (vinyl alcohol) polymers for advanced shielding applications. J. Polym. Res. 28, 1–10.

Alresheedi, M.T., Elsafi, M., Aladadi, Y.T., Abas, A.F., Ganam, A.B., Sayyed, M.I., Mahdi, M.A., 2023. Assessment of silicone rubber/lead oxide composites enriched with $\mathrm{Bi}_2\mathrm{O}_3$, WO_3 , BaO , and SnO_2 nanoparticles for radiation shielding applications. Polymers 15, 2160.

Alsafi, K., El-Nahal, M.A., Al-Saleh, W.M., Almutairi, H.M., Abdel-Gawad, E.H., Elsafi, M., 2024. Utilization of waste marble and Bi₂O₃ NPs as a sustainable replacement for lead materials for radiation shielding applications. Ceramics 7, 639–651

Alshahri, S., Alsuhybani, M., Alosime, E., Almurayshid, M., Alrwais, A., Alotaibi, S., 2021. LDPE/Bismuth oxide nanocomposite: preparation, characterization and application in X-ray shielding. Polymers 13, 3081. https://doi.org/10.3390/ polym13183081.

Ambika, M.R., Nagaiah, N., Harish, V., Lokanath, N.K., Sridhar, M.A., Renukappa, N.M., Suman, S.K., 2017a. Preparation and characterisation of isophthalic-Bi₂O₃ polymer composite gamma radiation shields. Radiat. Phys. Chem. 130, 351–358. https://doi.org/10.1016/j.radphyschem.2016.09.022.

Ambika, M.R., Nagaiah, N., Suman, S.K., 2017b. Role of bismuth oxide as a reinforcer on gamma shielding ability of unsaturated polyester based polymer composites. J. Appl. Polym. Sci. 134. https://doi.org/10.1002/app.44657.

Azman, N.Z., Siddiqui, S.A., Hart, R., Low, I.M., 2013. Effect of particle size, filler loadings and x-ray tube voltage on the transmitted x-ray transmission in tungsten oxide—epoxy composites. Appl. Radiat. Isot. 71, 62–67. https://doi.org/10.1016/j.apradiso.2012.09.012.

- Bawazeer, O., Makkawi, K., Aga, Z.B., Albakri, H., Assiri, N., Althagafy, K., Ajlouni, A.-W., 2023. A review on using nanocomposites as shielding materials against ionizing radiation. Journal of Umm Al-Qura University for Applied Sciences, 0123456789. https://doi.org/10.1007/s43994-023-00042-9.
- Berger, M.J., Hubbell, J.H., Seltzer, S.M., Chang, J., Coursey, J.S., Sukumar, R., Zucker, D.S., Olsen, K., 2010. XCOM: photon cross sections database. NIST Standard Reference Database (XGAM). https://www.nist.gov/pml/xcom-photon-crosssections-database.
- Bijanu, A., et al., 2022. Chemically bonded tungsten-based polymer composite for X-rays shielding applications. Mater. Today Commun. 32, 104100.
- Boubeta, M., et al., 2010. Self-assembled multifunctional Fe/MgO nanospheres for magnetic resonance imaging and hyperthermia. Nanomed. Nanotechnol. Biol. Med. 6, 362–370
- Çağlar, M., Kayacık, H., Karabul, Y., Kılıç, M., Özdemir, Z.G., İçelli, O., 2019. Na₂Si₃O₇/ BaO composites for the gamma-ray shielding in medical applications: experimental, MCNP5, and WinXCom studies. Prog. Nucl. Energy 117, 103119.
- Cao, D., Yang, G., Bourham, M., Moneghan, D., 2020. Gamma radiation shielding properties of poly (methyl methacrylate)/Bi₂O₃ composites. Nucl. Eng. Technol. 52, 2613–2619. https://doi.org/10.1016/j.net.2020.04.026.
- Chalkidou, A., et al., 2011. In vitro application of Fe/MgO nanoparticles as magnetically mediated hyperthermia agents for cancer treatment. J. Magn. Magn Mater. 6, 775, 790
- Charkiewicz, A.E., Backstrand, J.R., 2020. Lead toxicity and pollution in Poland. Int. J. Environ. Res. Publ. Health 17, 4385. https://doi.org/10.3390/ijerph17124385.
- Deka, N., Bera, A., Roy, D., De, P., 2022. Methyl methacrylate-based copolymers: recent developments in the areas of transparent and stretchable active matrices. ACS Omega 7 (42), 36929–36944. https://doi.org/10.1021/acsomega.2c04564.
- Demirbay, T., Çağlar, M., Karabul, Y., Kılıç, M., İçelli, O., Özdemir, Z.G., 2019. Availability of water glass/Bi₂O₃ composites in dielectric and gamma-ray screening applications. Radiat. Eff. Defect Solid 174, 419–434.
- Di, D.R., He, Z.Z., Sun, Z.Q., Liu, J., 2012. A new nano-cryosurgical modality for tumor treatment using biodegradable MgO nanoparticles. Nanomed. Nanotechnol. Biol. Med. 8, 1233–1241.
- Dignam, T., Kaufmann, R.B., LeStourgeon, L., Brown, M.J., 2019. Control of lead sources in the United States, 1970-2017: public health progress and current challenges to eliminating lead exposure. J. Publ. Health Manag. Pract. 25 (Suppl. 1, Lead Poisoning Prevention), \$13–\$522. https://doi.org/10.1097/PHH.000000000000889.
- Eke, C., Agar, O., Segebade, C., Boztosun, I., 2017. Attenuation properties of radiation shielding materials such as granite and marble against γ-ray energies between 80 and 1350 keV. Radiochim. Acta 105. 851–863. https://doi.org/10.1515/ract-2016-2690.
- El-Khatib, A.M., Abbas, M.I., Elzaher, M.A., Badawi, M.S., Alabsy, M.T., Alharshan, G.A., Aloraini, D.A., 2019. Gamma attenuation coefficients of nano cadmium oxide/high density polyethylene composites. Sci. Rep. 9, 16012. https://doi.org/10.1038/ s41598.019.52220.7
- Gohil, S.V., Suhail, S., Rose, J., Vella, T., Nair, L.S., 2017. In: Bose, S., Bandyopadhyay, A. (Eds.), Chapter 8 Polymers and Composites for Orthopedic Applications. Academic Press, pp. 349–403. https://doi.org/10.1016/B978-0-12-802792-9.00008-2.
- Hannachi, E., Sayyed, M.I., Slimani, Y., Elsafi, M., 2024. Gamma radiation shielding efficiency of some different ceramic composites: a comparative study. Radiat. Phys. Chem. 220, 111695.
- Hashem, M., et al., 2017. Influence of titanium oxide nanoparticles on the physical and thermomechanical behavior of poly methyl methacrylate (PMMA): a denture base resin. Sci. Adv. Mater. 9 (6), 938–944.
- Idris, M.M., Olarinoye, I.O., Kolo, M.T., Ibrahim, S.O., Rilwan, U., Sayyed, M.I., 2025. A comparative study of the radiation dose response of (ZnO)x(TeO₂)1-x thin films for high energy X-ray application. Ceram. Int. https://doi.org/10.1016/j.ceramint 2025 03 290
- Johnson, T.E., Cember, H., 2017. Introduction to Health Physics, fifth ed. McGraw-Hill Education, New York.
- Kavun, Y., 2019. Examination of radiation absorption properties of Pb(NO₃)₂ doped wallpapers. Bitlis Eren Üniversitesi Fen Bilimleri Dergisi 1–6. https://doi.org/ 10.17798/bitlisfen.630618.
- Khalid, Y.K., Umaru, I., Idris, M.M., Rilwan, U., Guto, J.A., Sayyed, M.I., Maisalatee, A. U., Mundi, A.A., Mahmoud, K.A., 2025. Microstructural, thermal analysis, and gamma-ray shielding properties of bricks made of various local natural materials. Radiat. Phys. Chem., 112742 https://doi.org/10.1016/j.radphyschem.2025.112742.
- Khrenov, V., Schwager, F., Klapper, M., Koch, M., Mullen, K., 2007. Compatibilization of inorganic particles for polymeric nanocompo sites. Optimization of the size and the compatibility of ZnO particles. Polym. Bull. 58, 799–807.
- Klein, L.W., Miller, D.L., Balter, S., Laskey, W., Haines, D., Norbash, A., Mauro, M.A., Goldstein, J.A., 2009. Occupational health hazards in the interventional laboratory: time for a safer environment. Radiology 250, 538–544. https://doi.org/10.1148/ radiol.2502082558.
- Krishnamoorthy, K., et al., 2012. Antibacterial activity of MgO nanoparticles based on lipid peroxidation by oxygen vacancy. J. Nanoparticle Res. 14, 1063.
- Krzywy, I., Krzywy, E., Pastuszak-Gabinowska, M., Brodkiewicz, A., 2010. Lead-is there something to be afraid of? Ann. Acad. Med. Stetin 56, 118–128.
- Kucuk, N., Cakir, M., Isitman, N.A., 2013. Mass attenuation coefficients, effective atomic numbers and effective electron densities for some polymers. Radiat. Protect. Dosim. 153, 127–134. https://doi.org/10.1093/rpd/ncs091.
- Li, Q., Wei, Q., Zheng, W., Zheng, Y., Okosi, N., Wang, Z., Su, M., 2018. Enhanced radiation shielding with conformal light-weight nanoparticle-polymer composite. ACS Appl. Mater. Interfaces 10, 35510–35515. https://doi.org/10.1021/ acsami.8b10600.

- Li, R., Gu, Y., Wang, Y., Yang, Z., Li, M., Zhang, Z., 2017. Effect of particle size on gamma radiation shielding property of gadolinium oxide dispersed epoxy resin matrix composite. Mater. Res. Express 4, 035035. https://doi.org/10.1088/2053-1591/ aa6651
- Mazrani, W., McHugh, K., Marsden, P.J., 2007. The radiation burden of radiological investigations. Arch. Dis. Child. 92, 1127–1131. https://doi.org/10.1136/ adc.2006.101782
- Mehrara, R., Malekie, S., Kotahi, S.M.S., Kashian, S., 2021. Introducing a novel low energy gamma ray shield utilizing polycarbonate bismuth oxide composite. Sci. Rep. 11, 10614. https://doi.org/10.1038/s41598-021-89773-5.
- Mittal, V., 2015. Synthesis Techniques for Polymer Nanocomposites; Polymer Nano-, Micro- & Macrocomposites Series. Wiley-VCH, Weinheim, Germany
- More, C.V., Alsayed, Z., Badawi, M.S., Thabet, A.A., Pawar, P.P., 2021. Polymeric composite materials for radiation shielding: a review. Environ. Chem. Lett. 19, 2057–2090. https://doi.org/10.1007/s10311-021-01189-9.
- Mostafa, M.Y., Zakaly, H.M., Issa, S.A., Saudi, H.A., Henaish, A.M.A., 2022. Tailoring variations in the linear optical and radiation shielding parameters of PVA polymeric composite films doped with rare-earth elements. Appl. Phys. A 128 (3), 199.
- Müller, K., Bugnicourt, E., Latorre, M., Jorda, M., Echegoyen Sanz, Y., Lagaron, J.M., Miesbauer, O., Bianchin, A., Hankin, S., Bölz, U., Pérez, G., Jesdinszki, M., Lindner, M., Scheuerer, Z., Castelló, S., Schmid, M., 2017. Review on the processing and properties of polymer nanocomposites and nanocoatings and their applications in the packaging, automotive and solar energy fields. Nanomaterials 7 (4). https://doi.org/10.3390/nano7040074.
- Muthamma, M.V., Prabhu, S., Bubbly, S.G., Gudennavar, S.B., 2021. Micro and nano Bi_2O_3 filled epoxy composites: thermal, mechanical and γ -ray attenuation properties. Appl. Radiat. Isot. 174, 1080.
- Park, J., Hwang, Y., 2017. XRD analysis of polymeric structures in PMMA. Mater. Res. Express 4 (9), 095302.
- Pavlenko, V.I., Cherkashina, N.I., Yastrebinsky, R.N., 2019. Synthesis and radiation shielding properties of polyimide/Bi₂O₃ composites. Heliyon 5, e01703. https://doi. org/10.1016/j.heliyon.2019.e01703.
- Pituru, S.M., Greabu, M., Totan, A., Imre, M., Pantea, M., Spinu, T., Tancu, A.M.C., Popoviciu, N.O., Stanescu, I.-I., Ionescu, E., 2020. A review on the biocompatibility of PMMA- based dental materials for interim prosthetic restorations with a glimpse into their modern manufacturing techniques. Materials 13, 2894. https://doi.org/ 10.3390/mal3132894.
- Ravneet, K., Singh, K.P., Tripathi, S.K., 2020. Study of linear and non-linear optical responses of MoSe2–PMMA nanocomposites. J. Mater. Sci. Mater. Electron. 31, 19974–19988.
- Rilwan, U., Edeh, S.A., Idris, M.M., Fatima, I.I., Olukotun, S.F., Arinseh, G.Z., Bonat, P.Z., El-Taher, A., Mahmoud, K.A., Hanafy, T.A., Sayyed, M.I., 2025a. Influence of waste glass on the gamma-ray shielding performance of concrete. Ann. Nucl. Energy 210, 110876. https://doi.org/10.1016/j.anucene.2024.110876.
- Rilwan, U., Abdulazeez, M.A., Maina, I., Olasoji, O.W., Atef, El-Taher, Adeshina, I.S., Sayyed, M.I., 2025b. Sustainable gamma radiation shielding: coconut shell ash modified concrete for radiation protection applications. Journal of Radiation and Nuclear Applications 10 (1), 33.44. https://doi.org/10.1857/j.jrpa/100106
- Nuclear Applications 10 (1), 33–44. https://doi.org/10.18576/jrna/100106.

 Rilwan, U., Abdulazeez, M.A., Maina, I., Olasoji, O.W., El-Taher, A., Alhindawy, I.G.,
 Mahmoud, K.A., Sayyed, M.I., Elsafi, M., Rashad, M., Maghrbi, Y., 2025c. The use of
 coconut shell ash as partial replacement of cement to improve the thermal properties
 of concrete and waste management sustainability in Nigeria and Africa, for radiation
 shielding application. Sci. Afr. 27, e02578. https://doi.org/10.1016/j.sciaf.2025.
- Rilwan, U., Abdulazeez, M.A., Maina, I., Olasoji, O.W., El-Taher, A., Maisalatee, A.U., Sarki, M.U., Mohammed, G., Sayyed, M.I., 2025d. Feasibility study on the possibility of utilizing e-nut shell ashes for gamma-radiation protection application. Radiat. Phys. Chem. 233, 112748. https://doi.org/10.1016/j.radphyschem.2025.112748.
- Rilwan, U., Aliyu, G.M., Olukotun, S.F., Idris, M.M., Mundi, A.A., Bello, S., Umar, I., El-Taher, A., Mahmoud, K.A., Sayyed, M.I., 2024. Recycling and characterization of bone incorporated with concrete for gamma-radiation shielding applications. Nucl. Eng. Technol. https://doi.org/10.1016/j.net.2024.02.045.
- Rotkovich, A.A., Tishkevich, D.I., German, S.A., Bondaruk, A.A., Dashkevich, E.S., Trukhanov, A.V., 2024. A study of the morphological, structural, and shielding properties of epoxy-W composite materials. Nexus of Future Materials 1, 13–19. https://nfmjournal.com/articles/5.
- Saleh, I.H., Ibrahim, N.M., Hassaan, M.A., Ghatass, Z.F., Arayro, J., Mezher, R., Ibosayyed, M., Elsafi, M., 2024. Using 7Be and 137Cs for assessing the land stability of alexandria region, Egypt. Sustainability 16, 1692.
- Saudi, H.A., Gomaa, H.M., El-Mosallamy, E.S.H., Elkatlawy, S.M., 2021. Optimal radiation shielding capacity and thermal properties of poly(methyl methacrylate) films enhanced with different metal complexes. Polym. Polym. Compos. 29 (9), S223–S228. https://doi.org/10.1177/0967391121998490.
- Sayyed, M.I., Al-Ghamdi, H., Almuqrin, A.H., Yasmin, S., Elsafi, M., 2022. A study on the gamma radiation protection effectiveness of nano/micro-MgO-reinforced novel silicon rubber for medical applications. Polymers 14, 2867. https://doi.org/ 10.3390/polym14142867.
- Sayyed, M.I., Almuqrin, A.H., Elsafi, M., Rilwan, U., 2024a. Evaluation of incorporation of granite waste and SnO2-NPs into coating mortar for gamma-ray shielding. Radiat. Phys. Chem. https://doi.org/10.1016/j.radphyschem.2024.111818.
- Sayyed, M.I., Rilwan, U., Mahmoud, K.A., Elsafi, M., 2024b. Experimental study of the radiation shielding characteristics of new PbO-Nagaro glasses. Nucl. Eng. Technol. https://doi. org/10.1016/j.net.2024.01.058.
- Sayyed, M.I., Almuqrin, A.H., More, C.V., Rilwan, U., Rashad, M., Elsafi, M., 2024c. Exploring gamma radiation shielding: the role of BaO in borosilicate glasses. Silicon. https://doi.org/10.1007/s12633-024-03045-1.

- Shahzad, K., Kausar, A., Manzoor, S., Rakha, S.A., Uzair, A., Sajid, M., Arif, A., Khan, A. F., Diallo, A., Ahmad, I., 2022. Views on radiation shielding efficiency of polymeric composites/nanocomposites and multi-layered materials: current state and advancements. Radiation 3, 1–20. https://doi.org/10.3390/radiation3010001.
- Stelzig, S.H., Klapper, M., Mullen, K., 2008. A simple and efficient route to transparent nanocomposites. Adv. Mater. 20 (5), 929–932.
- Subedi, B., Lamichhane, T.R., 2023. Radiation shielding properties of low-density Tibased bulk metallic glass composites: a computational study. Phys. Scri. 98 (3), 035003.
- Surung, B.S., Lokhande, R.M., Pawar, P.P., 2016. Linear attenuation coefficient and mean free path in the energy range of 0.1 MeV to 1.5 MeV. International Journal of Applied Research 2, 279–283. www.allresearchjournal.com.
- Tokar, E.J., Boyd, W.A., Freedman, J.H., Waalkes, M.P., 2013. Toxic effects of metals. In: Klaassen, C.D. (Ed.), Casarett and Doull's Toxicology: the Basic Science of Poisons, eighth ed. McGraw Hill https://accesspharmacy.mhmedical.com/content.aspx?boo kid=958§ionid=53483748.
- Wani, A.L., Ara, A., Usmani, J.A., 2015. Lead toxicity: a review. Interdiscip. Toxicol. 8, 55–64. https://doi.org/10.1515/intox-2015-0009.

- Wasel, O., Freeman, J., 2018. Comparative assessment of tungsten toxicity in the absence or presence of other metals. Toxics 6, 66. https://doi.org/10.3390/toxics6040066.
- Yasmin, S., Saifuddin, M., Chakraborty, S.R., Meaze, A.H., Barua, B.S., 2024. Evaluation of TeO₂-WO₃-Bi₂O₃ glasses for their potential in radiation shielding with the utilization of the Phy-X software program. Nexus of Future Materials 1, 51–55. https://www.nfmjournal.com/articles/9.
- Yousefi, F., Mousavi, S.B., Heris, S.Z., Naghash-Hamed, S., 2023. 2UV-shielding properties of a cost-effective hybrid PMMA-based thin film coatings using TiO₂ and ZnO nanoparticles: a comprehensive evaluation. Sci. Rep. 13 (1), 7116.
- Zhou, Q., Shang, Z., 2023. CuInS₂ nanocrystals embedded PMMA composite films: adjustment of polymer molecule weights and application in remote-type white LEDs. Nanomaterials 13, 1085. https://doi.org/10.3390/nano13061085.
- Rilwan, U., Abdulazeez, M.A., Maina, I., Olasoji, O.W., Olukotun, S.F., El-Taher, A., Sayyed, M.I., Chenko, G.Y.Nimchang, Jibr Ahmed, Guto, Adeyeba, O.A., Marashdeh, M.W., 2025e. Gamma Radiation Shielding and Thermal Performance of Concrete with Coconut Shell Ash Replacement. NIPES-Journal of Science and technology Research 7 (2), 354–362. https://doi.org/10.37933/nipes/7.2.2025.27.